

## Article

## A cost-effective force field tailored for solid-phase simulations of OLEDs materials

Mónica Moral, Wonjoon Son, Yoann Olivier, Juan-Carlos Sancho-García, and Luca Muccioli

*J. Chem. Theory Comput.*, **Just Accepted Manuscript** • DOI: 10.1021/acs.jctc.5b00164 • Publication Date (Web): 12 Jun 2015Downloaded from <http://pubs.acs.org> on June 16, 2015

### Just Accepted

“Just Accepted” manuscripts have been peer-reviewed and accepted for publication. They are posted online prior to technical editing, formatting for publication and author proofing. The American Chemical Society provides “Just Accepted” as a free service to the research community to expedite the dissemination of scientific material as soon as possible after acceptance. “Just Accepted” manuscripts appear in full in PDF format accompanied by an HTML abstract. “Just Accepted” manuscripts have been fully peer reviewed, but should not be considered the official version of record. They are accessible to all readers and citable by the Digital Object Identifier (DOI®). “Just Accepted” is an optional service offered to authors. Therefore, the “Just Accepted” Web site may not include all articles that will be published in the journal. After a manuscript is technically edited and formatted, it will be removed from the “Just Accepted” Web site and published as an ASAP article. Note that technical editing may introduce minor changes to the manuscript text and/or graphics which could affect content, and all legal disclaimers and ethical guidelines that apply to the journal pertain. ACS cannot be held responsible for errors or consequences arising from the use of information contained in these “Just Accepted” manuscripts.

# A cost-effective force field tailored for solid-phase simulations of OLEDs materials

M. Moral,<sup>†</sup> W.-J. Son,<sup>‡</sup> J. C. Sancho-García,<sup>†</sup> Y. Olivier,<sup>¶</sup> and L. Muccioli<sup>\*,§,||</sup>

*Departamento de Química Física, Universidad de Alicante, 03080 Alicante, Spain,  
Samsung Advanced Institute of Technology, Suwon, 443-803 Gyeonggi-do, South Korea,  
Laboratory for Chemistry of Novel Materials, University of Mons, 7000 Mons, Belgium,  
Department of Industrial Chemistry “Toso Montanari”, University of Bologna, 40136  
Bologna, Italy, and Laboratoire de Chimie des Polymères Organiques (LCPO), UMR 5629,  
University of Bordeaux, 33607 Pessac, France*

E-mail: Luca.Muccioli@u-bordeaux.fr

## Abstract

A united atom force field is empirically derived by minimizing the difference between experimental and simulated crystal cells and melting temperatures for eight compounds representative of organic electronic materials used in OLEDs and other devices: biphenyl, carbazole, fluorene, 9,9'-(1,3-Phenylene)bis(9H-carbazole) 1,3-bis(N-carbazolyl)benzene (mCP), 4,4'- Bis(N-carbazolyl)-1,1'-biphenyl (pCBP), phenazine, phenylcarbazole, and triphenylamine. The force field is verified against dispersion-corrected DFT calculations and shown to successfully reproduce the crystal struc-

---

\*To whom correspondence should be addressed

<sup>†</sup>Departamento de Química Física, Universidad de Alicante, 03080 Alicante, Spain

<sup>‡</sup>Samsung Advanced Institute of Technology, Suwon, 443-803 Gyeonggi-do, South Korea

<sup>¶</sup>Laboratory for Chemistry of Novel Materials, University of Mons, 7000 Mons, Belgium

<sup>§</sup>Department of Industrial Chemistry “Toso Montanari”, University of Bologna, 40136 Bologna, Italy

<sup>||</sup>Laboratoire de Chimie des Polymères Organiques (LCPO), UMR 5629, University of Bordeaux, 33607 Pessac, France

1  
2  
3  
4  
5  
6  
7  
8  
9  
10  
11  
12  
13  
14  
15  
16  
17  
18  
19  
20  
21  
22  
23  
24  
25  
26  
27  
28  
29  
30  
31  
32  
33  
34  
35  
36  
37  
38  
39  
40  
41  
42  
43  
44  
45  
46  
47  
48  
49  
50  
51  
52  
53  
54  
55  
56  
57  
58  
59  
60

ture also for two larger compounds employed as hosts in phosphorescent and thermally activated delayed fluorescence OLEDs: N,N'-Di(1-naphthyl)-N,N'-diphenyl-(1,1'-biphenyl)-4,4'-diamine (NPD), 1,3,5-tri(1-phenyl-1H-benzo[d]imidazol-2-yl)phenyl (TPBI).

The good performances of the force field, coupled to the large computational saving granted by the united atom approximation, make it an ideal choice for the simulation of the morphology of emissive layers for OLED materials in crystalline or glassy phases.

## 1 Introduction

Molecular and polymeric materials composed by recurrent aromatic moieties, such as phenyl and carbazolyl, are becoming ubiquitous in organic electronics applications:<sup>1</sup> as donors and acceptors for organic solar cells,<sup>2,3</sup> metal-free dyes<sup>4,5</sup> or hole transporters<sup>6</sup> in Graetzel solar cells, host semiconducting<sup>7-12</sup> and emitting materials in organic light-emitting diodes (OLEDs),<sup>9,13-17</sup> to name the most important ones. In particular all the emissive, hole and electron conducting (blocking) layers in small molecule and polymer OLEDs are often composed by nitrogen-rich units featuring a sp<sup>2</sup> or sp<sup>3</sup>-hybridized nitrogen (e.g. carbazoles and amines).<sup>7,18</sup>

To rationally improve the efficiency of the emissive layer, in particular to gain insight into the interplay between the host and guest electronic structures and consequently access to the rates governing hole-electron recombination and light emission processes, atomistic-like simulations combined with quantum chemistry calculations represent the most powerful theoretical method currently available.<sup>19,20</sup> However, high computational costs associated with such methodologies prevented so far their application to the chemically detailed simulation of an OLED, which are typically modeled only at macroscopic<sup>21</sup> or lattice level.<sup>22,23</sup>

Indeed, to investigate microscopically how structure affects kinetic and energetic magnitudes determining the efficiency in organic electronic devices, it is urgent to derive and employ force fields not only reliably reproducing the physical properties of these materials, but also simple

1  
2  
3  
4 and efficient enough to grant the possibility of simulating the morphology of a whole emissive  
5 layer,<sup>19,20,24,25</sup> i.e. of samples with dimensions of about  $10^4 - 10^6$  nm<sup>3</sup>. Note that the most  
6  
7 popular ones are optimized for other purposes<sup>26</sup> and that, to date, the literature appears to  
8  
9 be not only scarce of efforts for obtaining the first objective, exception made for the notable  
10  
11 work of Andrienko, Lennartz, Wenzel and collaborators,<sup>19,20,24,27-30</sup> but also almost absent  
12  
13 of attempts of reducing the computational cost via the derivation of simpler potentials.

14  
15 In the following, we thus try to partially fill this gap by describing and tailoring a simple  
16  
17 and computationally cost-effective united atom force field, able to reproduce rather accu-  
18  
19 rately the solid phase properties of some typical organic compounds employed in OLED  
20  
21 industry (Figure 1). The investigation is particularly timely because of the rise, besides  
22  
23 transition metal-based phosphorescent emitters, of new all-organic ones with thermally ac-  
24  
25 tivated<sup>12,13,31-35</sup> and aggregation induced fluorescence<sup>14-16,36</sup> playing a major role, that are  
26  
27 going to consent the realization of fully organic OLEDs, and represents the ideal prosecution  
28  
29 of our previous study on the accurate theoretical calculation of singlet-triplet energy gaps  
30  
31 for this class of materials.<sup>34</sup>

## 32 33 34 35 36 37 38 39 40 41 42 43 44 45 46 47 48 49 50 51 52 53 54 55 56 57 58 59 60

## 2 Molecules and force field initial setup

We started by selecting eight small molecules of known crystal cell structure, shown in Figure  
1: biphenyl (BPH), carbazole (CBZ), fluorene (FLU), 1,3-bis(carbazol-9-yl)benzene (mCP),  
4,4'-dicarbazole-1,1'-biphenyl (CBP), phenazine (PHE), phenylcarbazole (PCZ) and triph-  
enylamine (TPA)<sup>37</sup>. All these molecules are either used as host OLED materials themselves  
(e.g. PCZ, TPA, CBP), or constitute recurring chemical units in more complex polymeric or  
molecular structures.<sup>18,38</sup> We then proceeded to the setup of a united atom (UA) force field  
able to adequately reproduce the crystal structure of the selected compounds. The choice of  
a UA representation, also known as “extended atom” approximation, is justified by the large  
saving of computational time it allows, at the cost of a minimal loss of accuracy and of some

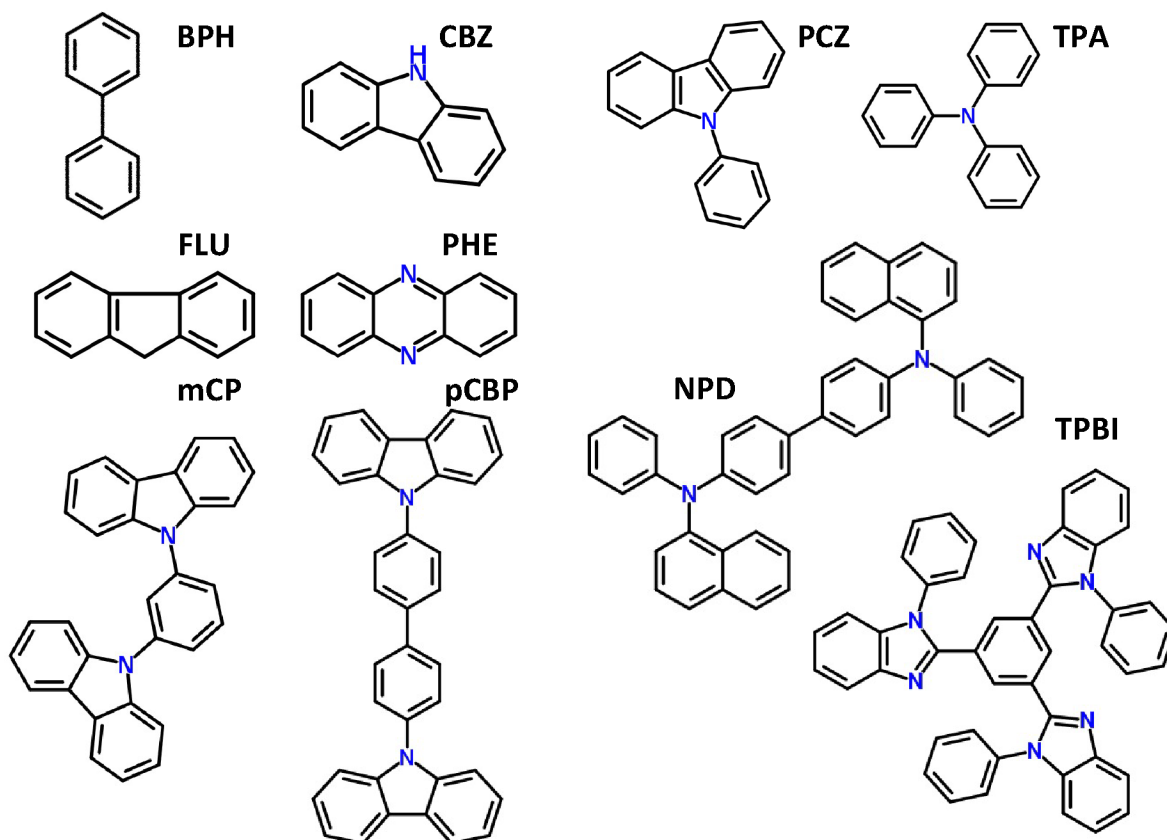


Figure 1: Chemical structures of the compounds studied: biphenyl (BPH), carbazole (CBZ), fluorene (FLU), 9,9'-(1,3-Phenylene)bis(9H-carbazole) 1,3-bis(N-carbazolyl)benzene (mCP), 4,4'-Bis(N-carbazolyl)-1,1'-biphenyl (pCBP), phenazine (PHE) 9-Phenyl-9H-carbazole (PCZ), and triphenylamine (TPA) compose the training set used for the empirical parameterization, while N,N'-Di(1-naphthyl)-N,N'-diphenyl-(1,1'-biphenyl)-4,4'-diamine (NPD), 1,3,5-tri(1-phenyl-1H-benzo[d]imidazol-2-yl)phenyl (TPBI) were simulated only to test the optimized version of the force field. The H atoms and the corresponding C-H bonds are omitted for clarity.

extra effort in its parameterization.<sup>39</sup> In a nutshell, every aliphatic or aromatic hydrogen atom is modelled only implicitly<sup>40</sup> and its mass is summed to the one of carbon atom it is bonded to. Such a customization of the force field can indeed turn into a long exercise requiring several steps.<sup>41</sup> Here we started with adopting the widely used AMBER-like or CHARMM-like potential energy function:<sup>42</sup>

$$\begin{aligned}
 U_{\text{total}} = & \sum_{\text{bonds}} K_r^* (r - r_e^*)^2 + \sum_{\text{angles}} K_\theta^* (\theta - \theta_e^*)^2 + \\
 & \sum_{\text{dihed}} \sum_{n^*} V_n^* [1 + \cos(n^* \phi + \gamma_n^*)] + \sum_{\text{improper}} K_\phi^* (\phi - \phi_e^*)^2 + \\
 & \sum_{\text{atoms}} \left\{ 4 \sqrt{\epsilon_i^* \epsilon_j^*} \left[ \left( \frac{\sigma_i^* + \sigma_j^*}{2r_{ij}} \right)^{12} - \left( \frac{\sigma_i^* + \sigma_j^*}{2r_{ij}} \right)^6 \right] + \frac{q_i^* q_j^*}{r_{ij}} \right\}. \quad (1)
 \end{aligned}$$

where for clarity all the parameters have been starred. For the harmonic constants  $K_r$  and  $K_\theta$  we rely on the AMBER95 parameter set,<sup>43</sup> while the corresponding equilibrium distances and angles  $r_e$  and  $\theta_e$  were adjusted comparing the equilibrium molecular mechanics geometries with the ones produced by highly accurate calculations. The torsional parameters  $V_n$ ,  $n$ ,  $\gamma_n$  were borrowed from the AMBER95 dataset for what concerns the rigid ones, e.g. torsions involving carbon atoms belonging to the same aromatic ring, while soft, anharmonic torsions were here parametrized with quantum chemistry calculations<sup>29,41,44</sup> at PBE0-D3(BJ)/def2-TZVP level. In practice, only three types of torsion were reworked: phenyl-phenyl, phenyl-carbazole, and the improper torsion involving the out-of-plane vibration of  $sp^2$  nitrogen; the phenyl-nitrogen torsion in TPA being modeled with standard parameters, as it is dominated by steric repulsion which confers it a propeller-like structure.<sup>45</sup> Fully relaxed scans of the potential energy surface as a function of the dihedral angle were run in steps of 5 degrees, using BPH and PCZ as target fragments, with the obtained profiles shown in Figure 2. It is worth noting that these torsions are present also in the largest compounds of the training set, namely mCP and pCBP, and in many other OLED materials.<sup>18,38</sup>

The force field parameters matching the torsional potentials were optimized with the pro-

cedure described in reference,<sup>44</sup> consisting in deriving the free energy torsional profile with adaptive biasing force MD runs<sup>46</sup> and fitting the difference between QM and MD with a cosine series (see eq 1). Turning to the Lennard-Jones (LJ) parameters  $\sigma_i$  and  $\epsilon$  entering the last term of eq 1, nine atom types were first identified (i. e. chemically equivalent atoms sharing the same parameters, see Tables 1 and 2) and their initial values was set to the one found in literature references.<sup>43,47-49</sup> As it is customarily done,<sup>42,50</sup> the atomic charges  $q$  were derived by fitting the molecular electrostatic potential obtained by quantum chemistry calculations. For this purpose the PBE0-D3(BJ)/def2-TZVP model chemistry was adopted,<sup>51-55</sup> with numerical thresholds systematically increased with respect to defaults, and dispersion corrections -D3(BJ),<sup>56</sup> because as we have reported recently, it shows good all-around performances for some of the compounds studied here, as well as for some emitters exhibiting thermally activated delayed fluorescence (see reference<sup>34</sup> for further details). Molecular geometries were first optimized by PBE0/def2-TZVP calculations, and then the charges on the heavy atoms were calculated at PBE0/TZVP level with the electrostatic potential fitting algorithm<sup>57</sup> implemented in the GAUSSIAN09 package.<sup>58</sup> All the other quantum mechanics calculations were performed with the ORCA code, version 3.0.0.<sup>59</sup> All the atomistic simulations were run with the NAMD 3.0 software.<sup>60</sup> The trajectories were analyzed with a in-house written Fortran 95 code.

Table 1: Atom types included in the force field and their occurrence for each molecule of the training set.

name	description	BPH	CBZ	FLU	mCP	pCBP	PHE	PCZ	TPA
C2	-CH <sub>2</sub> - group	-	-	1	-	-	-	-	-
CA	aromatic C	-	2	2	4	4	4	4	-
CH	ua aromatic C-H group	10	8	8	16	28	8	11	15
CX	bridge aromatic C	2	2	2	4	6	-	-	-
CY	aromatic C bonded to sp <sup>2</sup> N	-	-	-	2	2	-	1	3
N	aromatic sp <sup>2</sup> N	-	-	-	-	-	2	-	-
NH	carbazole NH group	-	1	-	-	-	-	-	-
N3	sp <sup>2</sup> N (e.g. in PCZ)	-	-	-	2	2	-	1	-
N4	triphenylamine sp <sup>3</sup> N	-	-	-	-	-	-	-	1

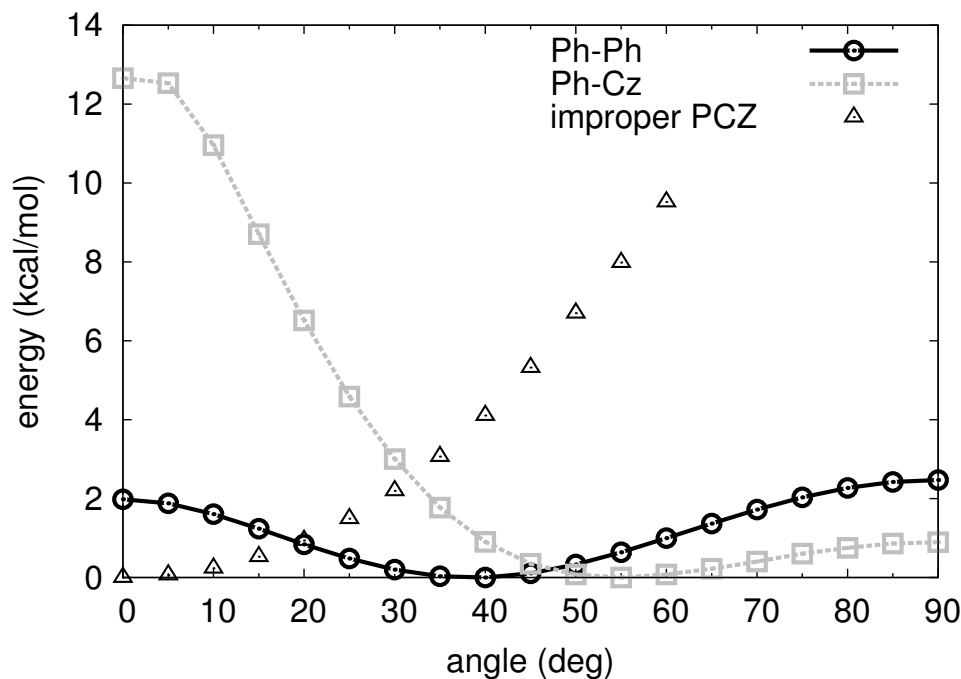


Figure 2: Quantum mechanical potential for the phenyl-phenyl dihedral angle in BPH (circles), for the phenyl-carbazole dihedral angle in PCZ (squares), and for the improper dihedral carbazole-N-phenyl in PCZ (triangles), systematically calculated at the PBE0-D3(BJ)/def2-TZVP level<sup>34</sup> by fully relaxing the geometry while keeping fixed the dihedral angle.

Table 2: Starting values of Lennard-Jones parameters  $\sigma$  (Å) and  $\epsilon$  (kcal/mol) for each atom type and corresponding reference (“start” force field), and percentage variation of the radii  $\sigma$  for the heuristic R1, R2, and R3 force fields.

name	$\sigma$	$\epsilon$		R1	R2	R3
C2	3.70	0.1094	<sup>48</sup>	+10%	+10%	+10%
CA	3.43	0.0860	<sup>50</sup>	+2%	+4%	+4%
CH	3.56	0.1114	<sup>49</sup>	+3%	+4%	+4%
CX	3.43	0.0860	<sup>50</sup>	-	-4%	-4%
CY, CW	3.43	0.0860	<sup>50</sup>	+4%	+4%	+5%
N	3.28	0.1700	<sup>50</sup>	+5%	+4%	-
NH	3.28	0.1700	<sup>50</sup>	+5%	+4%	+4%
N3	3.28	0.1700	<sup>50</sup>	+5%	+4%	+4%
N4, N5 <sup>61</sup>	3.28	0.1700	<sup>50</sup>	+5%	+4%	-



### 3 Computational strategy

For each target compound, a supercell was created by replicating the experimental crystal cell along its axes  $a$ ,  $b$ ,  $c$ , to have thus at least three replica per side, and supercell sides the closest possible to 5 nm, in order to realize a sensible compromise between finite size effects and computational costs. With these criteria, the sample sizes range from approximately 6000 to 10000 atoms, corresponding to  $N=540$  (BPH,  $6 \times 9 \times 5$  supercell<sup>62</sup>), 756 (CBZ,  $7 \times 3 \times 9^{63}$ ), 756 (FLU  $7 \times 3 \times 9^{64}$ ), 288 (mCP,  $6 \times 4 \times 3^{65}$ ), 180 (pCBP,  $6 \times 3 \times 5^{66}$ ), 560 (PHE,  $7 \times 10 \times 4^{67}$ ), 360 (PCZ,  $3 \times 5 \times 3^{68}$ ), and 432 (TPA,  $3 \times 3 \times 3^{69}$ ) molecules per simulation box, respectively. For each parameter set, supercells were equilibrated with Molecular Dynamics at constant volume for 0.4 ns, then at atmospheric pressure for 2 ns, and finally density and box sizes were averaged over a further 1 ns-long run; the simple velocity scaling thermostat and Berendsen's barostat were used in all the runs. Simulated temperatures for each compound correspond to the ones of the measurement of experimental crystal structure as downloaded from the Cambridge Structural Database (CSD, entries BIPHEN04, CRBZOL04, FLUREN01, NEPWUB, KANYUU, PHENAZ04, PEMWEJ, ZZZJCQ01), typically room temperature (set to 293 K for BPH, FLU, PHE, PCZ, TPA) or below (168 K CBZ, 291 K mCP, 120 K pCBP), while the pressure is always fixed to 1 atm.

In order to be able to quantitatively compare the results of two different force fields, and eventually to systematically vary the FF parameters to match the experimental results, it is necessary to define an appropriate scoring function. Here, the deviation of the simulated cell from the experimental one was measured as

$$F = \frac{1}{2} (\Delta_{vol} + \Delta_{def}) \quad (2)$$

which accounts, through the function  $\Delta_{vol}$ , for the variation of the volume of the simulated cell (subscript  $s$ ) with respect to the experimental one (subscript  $e$ ), and for the deformation

of the cell shape through  $\Delta_{def}$ :

$$\Delta_{vol} = \frac{1}{3} \frac{|V_e - V_s|}{V_e} \quad (3)$$

$$\Delta_{def} = \frac{1}{3} \left[ \prod |\cos(\delta_e^i - \delta_s^i)|^{-1} \prod \left( 1 + \frac{|l_e^i - l_s^i|}{l_e^i} \right) - 1 \right] \quad (4)$$

where  $l^i = a, b, c$  and  $\delta^i = \alpha, \beta, \gamma$  are the crystal cell axes and angles, respectively, and  $V = abc\sqrt{1 - \cos^2 \alpha - \cos^2 \beta - \cos^2 \gamma + 2 \cos \alpha \cos \beta \cos \gamma}$  is the volume of the crystal unit cell. In order not to bias the scoring functions towards systems with smaller unit cells, for which the absolute variations of volume and cell sides are obviously smaller, both  $\Delta_{vol}$  and  $\Delta_{def}$  are dimensionless quantities. In practice,  $F$  is zero for a perfect agreement between experiment and simulation, is greater than zero otherwise, and for the simple case of an isotropic deformation of the experimental cell (i. e.  $l_s^i = \lambda l_e^i$ ), takes the value of  $|\lambda - 1|$  for  $\lambda \rightarrow 0$ ; hence, small values of  $F$  can be assimilated to the strain of the simulated cell with respect to the experimental one.<sup>70</sup>

## 4 Optimization of Lennard-Jones radii

In a classical force field, the intermolecular forces responsible for the cohesive energy in crystal phase are represented by a Lennard-Jones and an electrostatic term - see last summation in eq 1. Considering that atomic point charges are directly derived from DFT calculations, which are accurate enough in the description of the molecular charge density,<sup>71</sup> our empirical exploration was limited to optimizing the Lennard-Jones parameters ( $\epsilon$  and  $\sigma$ , see also Tables 1 and 2), that conversely are very difficult to evaluate accurately by purely theoretical means.<sup>72,73</sup>

With the initial parameter set taken from the literature and customized with QM charges and dihedrals, an average score of 0.027 is obtained, a rather unsatisfactory value as it translates in overestimations of the densities as large as 0.12 g/cm<sup>3</sup> with the exception of BPH.

1  
2  
3 The observation of BPH being an outlier, which is confirmed for almost all the attempted  
4 parameterizations, it is not surprising as it is known that the intermolecular interactions for  
5 benzene and short oligophenyls are particularly difficult to model with classical, non polariz-  
6 able force fields<sup>74</sup> and special parameters are often required to obtain good accuracy.<sup>75,76</sup> In  
7 addition, the united atom approximation, that eliminates the aliphatic hydrogens and their  
8 point charges, yielded to a poor description of the electric quadrupoles of phenyl rings.<sup>77</sup>

9  
10 Also the global overestimation of the densities with standard parameters can be easily ratio-  
11 nalized, recalling that the OPLS LJ parameters are optimized for the simulation of liquids,<sup>78</sup>  
12 and not for the solid state. To support this statement with an example, it is worth noticing  
13 that the LJ parameters reported in Table 2 gave satisfactory results in modeling the liq-  
14 uid crystal phases of metal-free phthalocyanines,<sup>79</sup> while conversely they yield a rather poor  
15 description of poly-3-hexyl-thiophene crystalline domains.<sup>80</sup> Interestingly, a similar overes-  
16 timation of the experimental density was observed for the latter system: in that case, the  
17 bias was corrected by increasing the  $\sigma$  of the aliphatic carbons of the hexyl chains by 8%.<sup>80</sup>  
18 Here we applied the same strategy: after having assessed that small variations of the various  
19  $\epsilon$  do not alter significantly the scoring function, as shown in Figure S1, we proceeded with  
20 a systematic increase of the atom sizes  $\sigma$  for the atom types in Table 1, starting from the  
21 most abundant ones (CA and CH).  
22  
23  
24  
25  
26  
27  
28  
29  
30  
31  
32  
33  
34  
35  
36  
37  
38  
39

40 From inspecting Figure 3 it can be appreciated how the strategy of progressively modifying  
41 the  $\sigma$  parameters is successful: while no improvement is obtained by decreasing  $\sigma$  for CA  
42 or CH, conversely an increase of 2-4 percent points significantly reduces the average score  
43 from the initial value of 0.027 to a more acceptable 0.018. It is also useful to observe in Fig-  
44 ure 3 (see also Figures S1 and S2) that the most important contribution to the total score  
45 comes from the anisotropic deformation term  $\Delta_{def}$ , which cannot be decreased as  $\Delta_{vol}$  by  
46 uniformly scaling all the atom sizes. Therefore, once this stage of optimization was reached,  
47 we started from the “CH +4%” force field and applied some heuristic changes to the other  
48 atom types radii, by considering the relative occurrence of the atom types (Table 1) and  
49  
50  
51  
52  
53  
54  
55  
56  
57  
58  
59  
60

the separate scores of the different molecules in the training set (see Figure S2), obtaining three refined parameterizations, labeled R1, R2, R3, detailed in Table 2. These attempts further reduced the score, namely to a minimum of about 0.013 for the R3 case, that was accordingly selected as force field of election for further optimization. As shown in Table 3, with this parameterization all the simulated cell parameters and densities, BPH excluded, are very close to their experimental counterparts (RMSD 0.32, 0.16, and 0.43 Å for  $a$ ,  $b$ , and  $c$ , and 0.026 g/cm<sup>3</sup> for density).

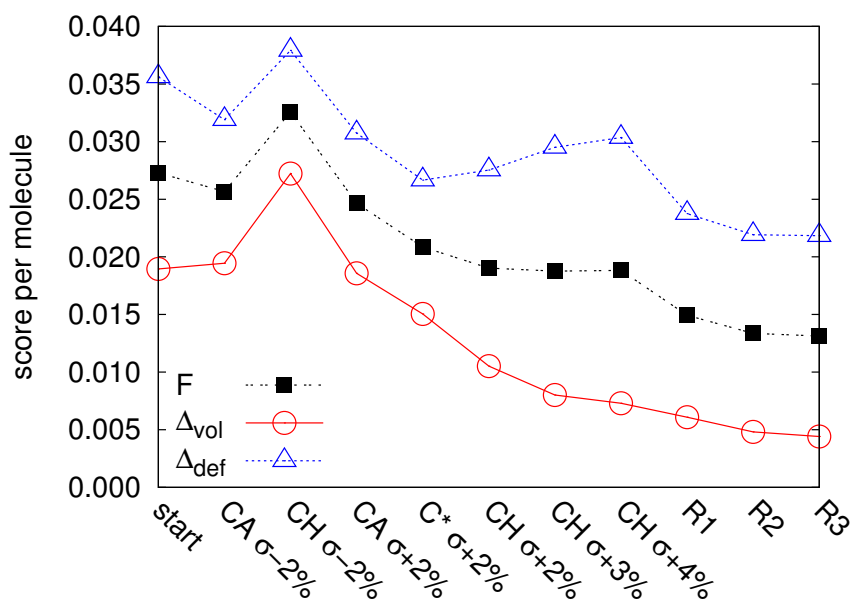


Figure 3: Performance of the different parameterizations obtained by varying the LJ radii. C\* stands for all carbon atom types. R1, R2, R3 are further refinements of the “CH  $\sigma$ +4%” force field, as described in the text.

## 5 Tuning of Lennard-Jones potential well depths

Following the observation that the structure of the crystal cell is only weakly influenced by changes of the potential well depth  $\epsilon$ , in the previous section we tackled next the optimization of the  $\sigma$  parameters for reproducing accurately the experimental crystal structures. However, at this stage the  $\epsilon$  values were left unoptimized, still demanding an alternative physical property for the purpose. With this purpose, we choose the melting points of the

Table 3: Experimental unit cells (e) and simulated ones (s) with the united atom R3 and R3  $\epsilon - 8\%$  force fields, and full atom FA (AMBER95 plus PBE0/def2-TZVP point charges) and T-FA force fields (identical to FA but with reparameterized dihedrals). Densities  $\rho$  are expressed in  $\text{g}/\text{cm}^3$ , cell volumes in  $\text{\AA}^3$ , sides in  $\text{\AA}$ , and angles in degrees. The angles, where equal to 90 degrees in the experimental cell, were kept fixed to this value during the simulation. The overall quality of the result is evaluated with the  $F$  score (eqs 2-4)

compound & FF		$\rho$	$V$	$a$	$b$	$c$	$\alpha$	$\beta$	$\gamma$	$F \cdot 10^2$
<b>BPH</b>	e	1.18	435.8	8.12	5.63	9.51	90.0	95.1	90.0	0.0
R3	s	1.12	460.5	8.64	5.67	9.38	90.0	95.5	90.0	2.4
R3 $\epsilon - 8\%$	s	1.10	470.0	8.89	5.60	9.42	90.0	95.6	90.0	3.2
FA	s	1.14	451.1	8.62	5.40	9.67	90.0	95.3	90.0	2.6
T-FA	s	1.15	449.9	8.54	5.43	9.68	90.0	95.3	90.0	2.3
<b>CBZ</b>	e	1.36	818.5	7.63	18.93	5.66	90.0	90.0	90.0	0.0
R3	s	1.34	827.0	7.63	18.73	5.78	90.0	90.0	90.0	0.7
R3 $\epsilon - 8\%$	s	1.34	827.8	7.62	18.74	5.79	90.0	90.0	90.0	0.8
<b>FLU</b>	e	1.20	917.6	8.47	18.92	5.72	90.0	90.0	90.0	0.0
R3	s	1.21	917.3	8.31	18.72	5.89	90.0	90.0	90.0	1.0
R3 $\epsilon - 8\%$	s	1.20	923.6	8.34	18.75	5.90	90.0	90.0	90.0	1.1
<b>mCP</b>	e	1.26	2159.7	9.07	12.50	19.04	90.0	90.0	90.0	0.0
R3	s	1.26	2161.7	9.59	12.40	18.17	90.0	90.0	90.0	1.9
R3 $\epsilon - 8\%$	s	1.25	2168.2	9.60	12.39	18.22	90.0	90.0	90.0	2.0
<b>pCBP</b>	e	1.31	1314.1	8.01	16.01	10.24	90.0	110.2	90.0	0.0
R3	s	1.34	1293.3	8.16	16.03	9.88	90.0	111.4	90.0	1.2
R3 $\epsilon - 8\%$	s	1.34	1295.9	8.16	16.03	9.90	90.0	111.3	90.0	1.1
FA	s	1.20	1420.2	8.42	14.97	11.26	90.0	109.3	90.0	5.2
T-FA	s	1.29	1373.9	9.47	14.63	9.91	90.0	114.9	90.0	6.3
<b>PHE</b>	e	1.33	460.1	7.08	5.07	12.79	90.0	102.3	90.0	0.0
R3	s	1.32	463.8	6.73	5.09	13.51	90.0	101.1	90.0	0.2
R3 $\epsilon - 8\%$	s	1.31	466.2	6.74	5.12	13.48	90.0	101.1	90.0	2.1
<b>PCZ</b>	e	1.22	2887.0	14.53	10.98	18.09	90.0	113.5	90.0	0.0
R3	s	1.24	2861.8	14.88	10.64	18.07	90.0	114.1	90.0	1.1
R3 $\epsilon - 8\%$	s	1.23	2876.9	14.90	10.67	18.09	90.0	114.1	90.0	1.0
FA	s	1.15	3126.9	16.24	10.53	18.28	90.0	116.1	90.0	4.3
T-FA	s	1.22	2868.6	14.48	10.54	18.79	90.0	112.5	90.0	1.5
<b>TPA</b>	e	1.18	5512.2	15.66	22.26	15.81	90.0	90.0	91.0	0.0
R3	s	1.19	5485.4	15.64	22.18	15.81	90.0	90.0	91.0	0.1
R3 $\epsilon - 8\%$	s	1.18	5538.9	15.73	22.17	15.88	90.0	90.0	91.0	0.3
<b>NPD</b>	e	1.23	1691.9	10.30	11.33	14.49	82.4	77.7	75.6	0.0
R3 $\epsilon - 8\%$	s	1.26	1649.4	10.18	11.42	14.18	82.3	77.5	75.8	1.1
<b>TPBI:CH<sub>3</sub>-OH</b>	e	1.25	3735.2	11.25	18.69	17.76	90.0	101.6	90.0	0.0
R3 $\epsilon - 8\%$	s	1.25	3722.2	11.01	18.23	18.54	90.0	100.9	90.0	1.6

1  
2  
3 target compounds, because they are a good indicator of intermolecular cohesion energy in  
4 the crystal, and attempted some scaling of the  $\epsilon$  to maximize the agreement with experiment.  
5  
6 A possible alternative would have been to choose boiling points, but the latter may not be  
7 available for the large compounds typically used in OLEDs, and in addition they are less rel-  
8 evant for OLED processing because often too high and far from room temperature. Melting  
9 points are straightforwardly determined with computer simulations by heating the crystal  
10 at increasing temperature until achieving the isotropic liquid phase, though hysteresis and  
11 system size may play an important role, typically leading to an overestimation of the actual  
12 melting temperature.<sup>81,82</sup> Here we used the supercells described in the previous sections as  
13 starting configurations, and equilibrated them for 3 ns at each simulated temperature and at  
14 atmospheric pressure. The temperature scan was performed at intervals of 25 K, typically  
15 starting at 300 K. As an operational definition of the melting point, the lowest temperature  
16 at which the sample becomes orientationally isotropic after 3 ns of simulation was consid-  
17 ered. An example of the typical characterization of the phase change in terms of density,  
18 orientational order parameter, translational diffusion coefficient and radial distribution is  
19 reported in the Supporting Information.  
20  
21  
22  
23  
24  
25  
26  
27  
28  
29  
30  
31  
32  
33  
34  
35

36 Clearly this is just a coarse measurement that is expected to produce an overestimation of  
37 melting points, because the interval of 25 K is rather large and the sampling time of 3 ns may  
38 be too short for the process to occur at temperatures close to the melting point. Once melting  
39 points were estimated, the performance of each force field were evaluated by means of the  
40 absolute deviation between experimental and simulated ones ( $|\Delta T| = \sum_{i=1}^8 |T_e^{m,i} - T_s^{m,i}|/8$ );  
41  
42 on the basis of the previous considerations on the melting point determination, any value  
43 below 50 K can be considered a very good score. In attempting this evaluation, it is also  
44 important to take into account that there is no guarantee that a classical force field able  
45 to reproduce simultaneously the experimental melting point and the crystal structure may  
46 exist: for instance, it may occur that by altering the  $\epsilon$ , also the crystal cell scoring function  
47  
48  
49  
50  
51  
52  
53  
54  
55  
56  
57  
58  
59  
60  
 $F$  could increase.

1  
2  
3 From Table 4, that resumes the scores for all the attempts of scaling  $\epsilon$  parameters, we observe  
4 that luckily it is not the case for changes up to 10% with respect to the initial values, but  
5 that on the other hand the melting point are largely overestimated by the force fields. The  
6 scores also show that all the variations of the R3 force field proposed here overestimate  
7 the boiling points of the target molecules, with the usual exception of BPH. In order to  
8 decrease the boiling points, the interaction between atoms must be decreased, and hence  $\epsilon$   
9 reduced, but with the constraint of not worsening the reproduction of experimental crystal  
10 structure, monitored through the  $F$  scoring function. In our case, we found that the best  
11 compromise is obtained with a scaling to 92% of the original interaction strengths (Table 2),  
12 and we finally labelled this force field as "R3  $\epsilon - 8\%$ ". By examining again the results  
13 presented in Table 3, it can be noticed that the performances are slightly lower than the  
14 ones of R3, while the melting temperatures obtained for the scaled force field are at least 20  
15 K closer to the experimental ones. Using this parameterization we also computed the surface  
16 energies for crystal (100), (010) and (001) planes, and for glassy samples obtained by freezing  
17 and equilibrating the liquid samples obtained above (see figure S5 and table S5 for further  
18 details). Such energies vary in a range between 0.05 and 0.15 J/m<sup>2</sup> for the crystal phase, in  
19 line with calculated<sup>83,84</sup> and experimental data<sup>85</sup> for other organic crystals. Conversely they  
20 are almost halved in glass phase (0.05-0.08 J/m<sup>2</sup>), reflecting the lower internal energy of the  
21 bulk glass phase with respect to the bulk crystal.  
22  
23  
24  
25  
26  
27  
28  
29  
30  
31  
32  
33  
34  
35  
36  
37  
38  
39  
40  
41  
42  
43  
44

## 45 **6 Additional tests for the intermolecular potential**

46  
47 As a further quality check of R3  $\epsilon - 8\%$  force field, we compared its prediction for selected  
48 intermolecular potential energy curves with the ones produced by state-of-the-art dispersion-  
49 corrected Density Functional Methods (DFT) methods,<sup>73</sup> with the latter specifically includ-  
50 ing the correct dependence on the internuclear separation at large distances; i.e., the so-called  
51 long-range behavior. We selected for this purpose the well-rounded Perdew-Burke-Ernzerhof  
52  
53  
54  
55  
56  
57  
58  
59  
60

Table 4: Melting points (K) for the studied compounds, as obtained by systematically rescaling the original LJ energy well depths  $\epsilon$  of all atom types, and using the radii of the R3 parameter set. The corresponding crystal structure score  $F$  and the mean absolute deviation between experimental and simulated melting temperatures ( $|\Delta T| = \sum_{i=1}^8 |T_e^{m,i} - T_s^{m,i}|/8$ , in K) are also reported.

compound	EXP <sup>86</sup>	R3	+10%	-5%	-8%	-10%	-15%	-20%
BPH	342	325	350	325	300	300	300	275
CBZ	518	700	750	675	675	650	625	600
FLU	386	550	600	525	525	500	500	475
mCP	449	725	775	700	700	700	650	650
pCBP	556	950	1050	900	875	850	825	775
PHE	447	650	675	625	600	600	575	550
PCZ	369	550	600	525	525	525	475	425
TPA	399	475	525	475	475	450	425	400
$ \Delta T $	0	187	232	165	162	149	124	102
$F \cdot 10^2$	0	1.31	1.32	1.34	1.44	1.90	1.92	2.05

(PBE) functional in its standard hybrid (PBE0) and revised (revPBE0) versions<sup>51–54</sup> with the rather large (nearly-converged) def2-TZVP basis set, while regarding the dispersion corrections, we employed either the -D3(BJ) function<sup>56</sup> or the -NL (van der Waals) approach,<sup>87</sup> to separately disentangling the effect (if any) of both the functional form and the dispersion correction used. In addition, we tested the (computationally inexpensive compared to other DFT-based methods) recently developed HF-3c method, which includes Kruse and Grimme’s geometric counterpoise corrections (gCP), the -D3(BJ) dispersion correction again, and a short-range basis incompleteness (SRB) correction for systematically overestimated bond lengths for electronegative elements when employing small basis sets.<sup>88</sup> The level of accuracy of the above theoretical methods was first verified by comparison with high level calculations published by Sherrill and coworkers by using accurate (nearly-converged) methods such as CCSD(T)/aug-cc-pVDZ, CCSD(T)/aug-cc-pVQZ, and MP2/aug-cc pVQZ, all of them including counterpoise correction (CP) to reduce as much as possible the well-known basis set incompleteness error typical of these calculations.<sup>89</sup> In particular, the classical cofacial and “T” geometries were explored for a pair of benzene molecules, and the corresponding intermolecular energies were calculated as function of the distance between the centers of



1  
2  
3  
4 mass of the two interacting molecules (figure 4). PBE0 and revPBE0 give very similar en-  
5  
6 ergies, while the choice of the dispersion correction, -D3(BJ) or -NL, seems more critical,  
7  
8 with -NL providing systematically weaker interaction energies with respect to -D3(BJ), and  
9  
10 getting thus closer to the CCSD(T) reference values. HF-3c is in line with the more accurate  
11  
12 methods for the T configuration, but instead largely overestimates the maximum interaction  
13  
14 energy and underestimates the distance at which the cofacial interaction is maximum. This  
15  
16 occurs also for PBE0 and revPBE0 calculations, for both benzene-benzene configurations,  
17  
18 but to a much lower extent, though not negligible in terms of percentage, in particular for  
19  
20 the energies (for all the values of “equilibrium” distances and energies, see additional tables  
21  
22 S1-S4 in the supporting information). It can then be preliminarily concluded that for small  
23  
24 aromatic molecules, dispersion-corrected PBE0/def2-TZVP calculations (independently of  
25  
26 the correction used) give semiquantitatively accurate results for energies, and quantitative for  
27  
28 distances, while the computationally cheaper HF-3c cannot be considered reliable enough,  
29  
30 at least for  $\pi$ -stacking energies, like in the case of the benzene cofacial dimer.

31  
32 We proceeded then to the evaluation of intermolecular energies for molecular pairs of BPH  
33  
34 and TPA (see supporting information for PCZ), in this case comparing quantum chemistry  
35  
36 calculations with molecular mechanics. These molecules, at their experimental geometry in  
37  
38 the crystal phase, were rotated into their principal inertial frame and superimposed. One of  
39  
40 them was kept fixed, while the second was moved along the three cartesian directions, corre-  
41  
42 sponding to the orientation of the inertia axes with increasing eigenvalue. Starting with the  
43  
44 extreme case of biphenyl (figure 5 left), we notice that all the quantum chemistry methods  
45  
46 give approximately the same prediction for the minimum energy distance, while both the  
47  
48 “start” and “R3  $\epsilon - 8\%$ ” provide a rather large underestimation (about 1 Å) for the  $x$  and  
49  
50  $y$  displacement directions. The rationale of this behaviour can be found in the united atom  
51  
52 approximation: as shown by the snapshots in figure 5 left, the  $x$  and  $y$  directions correspond  
53  
54 to hydrogen-hydrogen contacts. These hydrogen are not present in the united atom force  
55  
56 fields, where they are only partially compensated by a larger van der Waals radius on the  
57  
58  
59  
60

1  
2  
3  
4 corresponding carbon, hence these force fields underestimate the distance, and overestimate  
5 the interaction. As a further proof, we computed the same potential energy also with the  
6 standard AMBER95/OPLS full atom parameters (black two-dashed lines), which conversely  
7 adheres to the ab initio curves. On the contrary, the  $z$  ( $\pi$ -stacking) direction is not affected  
8 by the united atom approximation, and here both “start” and “R3  $\epsilon$ 8%” perfectly agree with  
9 DFT values, while as expected HF-3c, and more surprisingly AMBER95, overestimate the  
10 attraction between the two parallel BPH molecules. Moving to the larger and more isotropic  
11 TPA molecule, the curves in figure 5 right show that in this case united atom approximation  
12 is harmless and that the united atom FFs agrees with dispersion-corrected DFT values, while  
13 on the contrary HF-3c performs poorly, constantly overestimating the interaction energies.  
14 As a additional comment, it is worth noting that: i) the small differences between the “start”  
15 and “R3  $\epsilon$ 8%” FFs results are always comparable or lower than the differences between one  
16 dispersion-corrected DFT calculation and another, and ii) the very similar performance of  
17 the two FFs for the computation of interaction potential curves contrasts with their different  
18 capabilities of reproducing the crystal cells of the target compounds. It rather appears from  
19 these results that for the time being, DFT-derived potential energy curves cannot be used as  
20 a reference method for parameterizing force fields,<sup>90</sup> and that the empirical tuning remains  
21 a more viable way.

22  
23  
24 For achieving a further validation of the “R3  $\epsilon$  – 8%” FF parameters, we repeated the simu-  
25 lation scheme described in section 3 for two molecules outside the training set for which the  
26 experimental crystal structure is known: N,N'-bis(1-Naphthyl)-N,N'-diphenyl-1,1'-biphenyl-  
27 4,4'-diamine (NPD, 5 x 4 x 3 supercell,<sup>91</sup> N=120 molecules, 5520 centers, CSD entry RE-  
28 HJAQ01) and 2,2',2''-benzene-1,3,5-triyltris(1-phenyl-1H-benzimidazole) (TPBI, co-crystal  
29 with methanol, 4 x 3 x 3 supercell,<sup>92</sup> N=284 molecules for each species, 7776 centers, CSD  
30 entry QUCJAA). Again, wherever necessary, soft torsional potentials were re-parametrized  
31 (see figure S4), and united atom charges were calculated for each center for both molecules  
32 (see supporting information). In Table 3), it can be noticed that for these two example  
33  
34  
35  
36  
37  
38  
39  
40  
41  
42  
43  
44  
45  
46  
47  
48  
49  
50  
51  
52  
53  
54  
55  
56  
57  
58  
59  
60

1  
2  
3 molecules the quality of the reproduction of the experimental cells is good and compara-  
4 ble to the one achieved for the molecule belonging to the training set, suggesting that the  
5 Lennard-Jones parameters derived in this work could be safely transferred to other similar  
6 compounds.  
7  
8  
9

10  
11 To conclude, it is also worth assessing whether the parameterization exercise is just a con-  
12 sequence of opting for the united atom approximation, and also if this approximation is  
13 actually useful for saving precious computational time. For doing so, we chose the most  
14 complex molecule in the training set, pCBP, and set up a full atom force field by employing  
15 this time the full atom PBE0/def2-TZVP charges, and the popular GAFF parameters for  
16 Lennard-Jones and intramolecular parameters.<sup>50</sup> We produced two versions of this force field,  
17 one without re-optimizing the dihedral parameters (labelled FA in Table 3), and a second one  
18 (T-FA) where the phenyl-phenyl, phenyl-carbazole, and the improper sp<sup>2</sup> nitrogen dihedrals  
19 were refined with ab initio data, exactly as described above for the united atom FF. As this  
20 re-optimization requires the simulation of BPH and CBZ as well, we reported in Table 3  
21 also the results corresponding to their crystal cells. Starting with the difficult case of BPH,  
22 it appears that also the full atom picture does particularly improve the simulation results,  
23 independently on the dihedral potential: the density gets closer to the experimental one, but  
24 the value of *b* side decreases with respect to the experiment (and to the united atom FFs).  
25 For CBZ instead the reparametrization of the dihedral seems very relevant: the full atom *F*  
26 score drops from a very poor 0.043 to 0.015 because of that; however, the optimized united  
27 atom FFs perform slightly better. For pCBP the comparison is even more rewarding for the  
28 united atom force fields, which give scores of about 0.01 versus 0.05-0.06 for the full atom  
29 ones, thus confirming the necessity of tailoring the LJ parameters for solid state simulations.  
30 Finally, these tests provided us with an estimate of the computational savings brought by  
31 the united atom approximation, consisting in an appreciable factor of about six times (0.4  
32 days/ns vs 2.5 days/ns for pCBP on a single logical core of an Intel Xeon E5-2620v2 2.1GHz  
33 processor).  
34  
35  
36  
37  
38  
39  
40  
41  
42  
43  
44  
45  
46  
47  
48  
49  
50  
51  
52  
53  
54  
55  
56  
57  
58  
59  
60

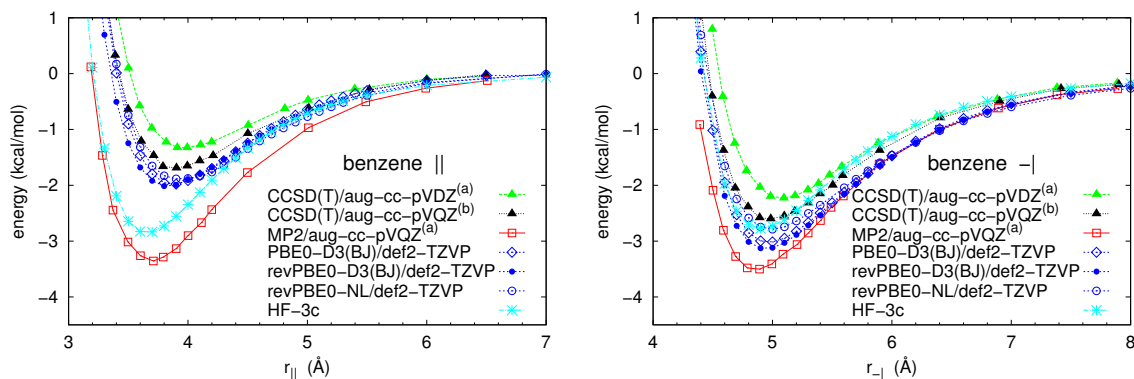


Figure 4: Calculated intermolecular energies for two cofacial (left) and “T” oriented (right) benzene molecules. MP2 and CCSD(T) data are extracted from reference.<sup>89</sup> (a) Counterpoise corrected values; (b) values estimated from counterpoise corrected CCSD(T)/aug-cc-pVDZ and MP2/aug-cc-pVDZ calculations.

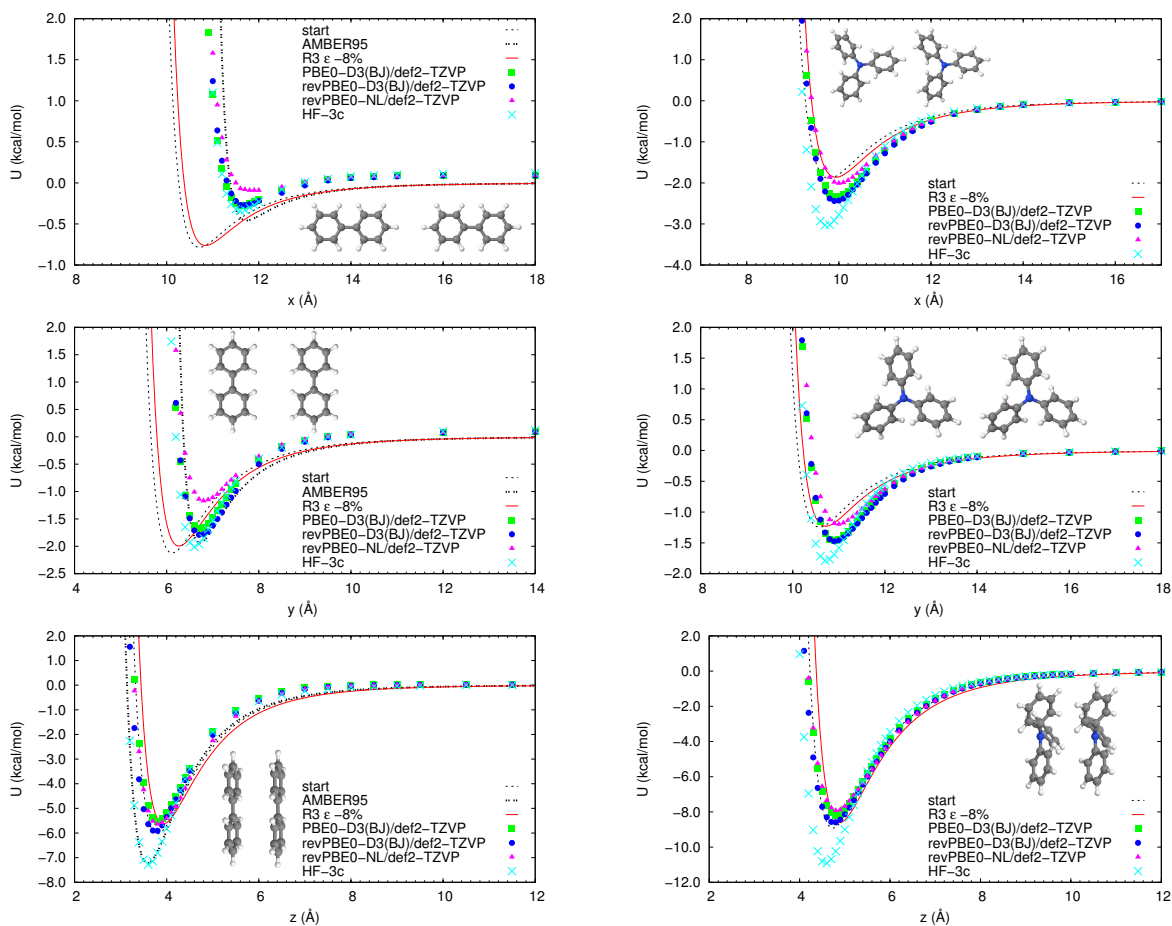


Figure 5: Calculated intermolecular energies for two parallel biphenyl molecules displaced along their  $x$ ,  $y$  and  $z$  inertia axes (left), and corresponding energies for two triphenylamine molecules (right).

## 7 Conclusions

In summary, we derived a simple molecular mechanics force field, aimed at the accurate and computationally efficient simulation of the morphology of materials used in the realization of organic light-emitting diodes. To increase the awareness of the potential users, we would like to recap here the main approximations, limitations, and good practices for a safe application of the force field parameters:

- the force field relies on the united atom approximation, where hydrogen are only implicitly accounted for: this grants a speed-up of about 600%, but also a lack of accuracy in describing specific contacts (see Figure 5), and cannot be used for hydrogen-bond forming systems.
- DFT calculations at the PBE0-D3(BJ)/def2-TZVP level were performed for the parameterization of the point charges on each united atom center, and for the soft torsional potentials between rigid aromatic units: similar calculations are required for any new compound to be studied.
- The Lennard-Jones parameters were empirically optimized in order to maximize the agreement with available experimental data, namely crystal cell shape and size, and the melting temperatures, for a training set of eight compounds.
- As the main empirical tuning of the parameters was performed to match the experimental crystal - hence a solid phase - we hypothesize that the parameterization will be effective also in reproducing another solid phase, the glassy one typically found in OLED devices.
- It is probably impossible to obtain a classical and simple force field “for all seasons”<sup>93</sup>- for instance, coarse-grained force fields for polymers work only close to the temperature and pressure they are derived,<sup>94</sup> and different force fields are required to reproduce high and low pressure benzene polymorphs.<sup>95</sup> In our specific case, reproduction of the

boiling point is not satisfactory, consequently we discourage the application of the force field for simulations of bulk liquid phases.

- The transferability of the force field was demonstrated by performing the simulation in crystal phase of two compounds outside the training set, which were again in good agreement with experiment. This result, although promising, is not sufficient to ensure the transferability to other compounds, in particular if containing new chemical moieties. In that case, the best practice would be to benchmark again the force field against the experimental crystal structure, if available, or versus any other experimental data.

Having listed all the limitations of the proposed methodology, it also is worth stressing that the good reproduction of physical properties in the solid state, together with the large computational saving expected with respect to full atom force fields, make the force field presented here a suitable candidate for the simulation of the morphology of emissive layers for OLED materials consisting of some thousands of molecules, paving the way towards their computational screening in a multi-scale approach.

## Acknowledgement

This work was supported by the Samsung Advanced Institute of Technology (SAIT)'s Global Research Outreach (GRO) Program. The research in Bordeaux has been funded by the French national grant ANR-10-LABX-0042-AMADEus managed by the National Research Agency under the initiative of excellence IdEx Bordeaux programme (reference ANR-10-IDEX-0003-02). The work in Mons was supported by the Programme d'Excellence de la Région Wallonne (OPTI2MAT project) and FNRS-FRFC.

## Supporting Information Available

Additional figures: S1) effect of scaling the Lennard-Jones  $\epsilon$  parameters on the scoring function, S2) compound-wise performances of the different parameterizations, S3) intermolecular

1  
2  
3 potential energy curves for PCB. S4) torsional energy profiles for NPD and TPBI specific  
4 dihedral angles. S5) Glass transition temperature determination for the target compounds  
5  
6  
7  
8 S6) Example of the characterization of the crystal-liquid phase transition. Tables with fit  
9 parameters of benzene, BPH, PCZ, and TPA intermolecular energies with Morse equation.  
10  
11 Table of calculated surface energies for crystalline and glassy samples. Archive containing:  
12  
13 CHARMM topology and parameter files (united atom R3  $\epsilon$ 8% and full atom T-FA), typical  
14  
15 NAMD configuration file, pdb files for united atom and full atom crystal cells. This material  
16  
17 is available free of charge via the Internet at <http://pubs.acs.org/>.  
18  
19

## 20 21 22 Notes and References

- 23  
24  
25 (1) Boudreault, P.-L. T.; Beaupre, S.; Leclerc, M. *Polym. Chem.* **2010**, *1*, 127–136.  
26  
27  
28 (2) Gendron, D.; Leclerc, M. *Energy Environ. Sci.* **2011**, *4*, 1225–1237.  
29  
30  
31 (3) Barito, A.; Sykes, M. E.; Huang, B.; Bilby, D.; Frieberg, B.; Kim, J.; Green, P. F.;  
32 Shtein, M. *Adv. Ener. Mater.* **2014**, *4*, 1400216.  
33  
34  
35 (4) Mishra, A.; Fischer, M. K. R.; Bäuerle, P. *Angew. Chem. Int. Ed.* **2009**, *48*, 2474–2499.  
36  
37  
38 (5) Yeh-Yung Lin, R.; Lin, H.-W.; Yen, Y.-S.; Chang, C.-H.; Chou, H.-H.; Chen, P.-W.;  
39 Hsu, C.-Y.; Chen, Y.-C.; Lin, J. T.; Ho, K.-C. *Energy Environ. Sci.* **2013**, *6*, 2477–2486.  
40  
41  
42  
43 (6) Zhou, N.; Lee, B.; Timalina, A.; Guo, P.; Yu, X.; Marks, T. J.; Facchetti, A.; Chang, R.  
44 P. H. *J. Phys. Chem. C* **2014**, *118*, 16967–16975.  
45  
46  
47  
48 (7) Yook, K. S.; Lee, J. Y. *Adv. Mater.* **2014**, *26*, 4218–4233.  
49  
50  
51 (8) Chen, D.; Su, S.-J.; Cao, Y. *J. Mater. Chem.* **2014**, *2*, 9565–9578.  
52  
53  
54 (9) Zhang, T.; Chu, B.; Li, W.; Su, Z.; Peng, Q. M.; Zhao, B.; Luo, Y.; Jin, F.; Yan, X.;  
55 Gao, Y.; Wu, H.; Zhang, F.; Fan, D.; Wang, J. *ACS Appl. Mater. Interfaces* **2014**, *6*,  
56  
57 11907–11914.  
58  
59  
60

- 1  
2  
3  
4 (10) He, X.; Cai, D.; Kang, D.-Y.; Haske, W.; Zhang, Y.; Zuniga, C. A.; Wunsch, B. H.;  
5 Barlow, S.; Leisen, J.; Bucknall, D.; Kippelen, B.; Marder, S. R. *J. Mater. Chem. C*  
6 **2014**, *2*.
- 7  
8  
9  
10 (11) Gaj, M. P.; Fuentes-Hernandez, C.; Zhang, Y.; Marder, S. R.; Kippelen, B. *Org. Elec-*  
11 *tron.* **2015**, *16*, 109 – 112.
- 12  
13  
14 (12) Suzuki, Y.; Zhang, Q.; Adachi, C. *J. Mater. Chem. C* **2015**, *3*, 1700–1706.
- 15  
16  
17 (13) Mayr, C.; Lee, S. Y.; Schmidt, T. D.; Yasuda, T.; Adachi, C.; Brütting, W. *Adv. Funct.*  
18 *Mater.* **2014**, *24*, 5232–5239.
- 19  
20  
21 (14) Gong, Y.; Liu, J.; Zhang, Y.; He, G.; Lu, Y.; Fan, W. B.; Yuan, W. Z.; Sun, J. Z.;  
22 Zhang, Y. *J. Mater. Chem.* **2014**, *2*, 7552–7560.
- 23  
24  
25 (15) Huang, J.; Sun, N.; Yang, J.; Tang, R.; Li, Q.; Ma, D.; Li, Z. *Adv. Funct. Mater.* **2014**,  
26 *24*, 7645–7654.
- 27  
28  
29 (16) Chen, L.; Jiang, Y.; Nie, H.; Hu, R.; Kwok, H. S.; Huang, F.; Qin, A.; Zhao, Z.;  
30 Tang, B. Z. *ACS Appl. Mater. Interfaces* **2014**, *6*, 17215–17225.
- 31  
32  
33 (17) Choi, E. Y.; Mazur, L.; Mager, L.; Gwon, M.; Pitrat, D.; Mulatier, J. C.; Monnereau, C.;  
34 Fort, A.; Attias, A. J.; Dorkenoo, K.; Kwon, J. E.; Xiao, Y.; Matczyszyn, K.; Samoc, M.;  
35 Kim, D.-W.; Nakao, A.; Heinrich, B.; Hashizume, D.; Uchiyama, M.; Park, S. Y.;  
36 Mathevet, F.; Aoyama, T.; Andraud, C.; Wu, J. W.; Barsella, A.; Ribierre, J. C. *Phys.*  
37 *Chem. Chem. Phys.* **2014**, *16*, 16941–16956.
- 38  
39  
40 (18) Yook, K. S.; Lee, J. Y. *Adv. Mater.* **2012**, *24*, 3169–3190.
- 41  
42  
43 (19) Baumeier, B.; May, F.; Lennartz, C.; Andrienko, D. *J. Mater. Chem.* **2012**, *22*, 10971–  
44 10976.
- 45  
46  
47 (20) Kordt, P.; van der Holst, J. J. M.; Al Helwi, M.; Kowalsky, W.; May, F.; Badinski, A.;  
48 Lennartz, C.; Andrienko, D. *Adv. Funct. Mater.* **2015**, *25*, 1955–1971.
- 49  
50  
51  
52  
53  
54  
55  
56  
57  
58  
59  
60



- 1  
2  
3  
4 (21) Perucco, B.; Reinke, N.; Rezzonico, D.; Knapp, E.; Harkema, S.; Ruhstaller, B. *Org.*  
5 *Electron.* **2012**, *13*, 1827 – 1835.  
6  
7  
8 (22) Mesta, M.; Carvelli, M.; de Vries, R. J.; van Eersel, H.; van der Holst, J. J. M.;  
9 Schober, M.; Furno, M.; Lüssem, B.; Leo, K.; Loebel, P.; Coehoorn, R.; Bobbert, P. A.  
10 *Nat. Mater.* **2013**, *12*, 652–658.  
11  
12  
13 (23) van Eersel, H.; Bobbert, P. A.; Janssen, R. A. J.; Coehoorn, R. *Appl. Phys. Lett.* **2014**,  
14 *105*, 143303.  
15  
16  
17 (24) Neumann, T.; Danilov, D.; Lennartz, C.; Wenzel, W. *J. Comput. Chem.* **2013**, *34*,  
18 2716–2725.  
19  
20  
21 (25) Ratcliff, L. E.; Grisanti, L.; Genovese, L.; Deutsch, T.; Neumann, T.; Danilov, D.; Wen-  
22 zel, W.; Beljonne, D.; Cornil, J. *J. Chem. Theory Comput.* 10.1021/acs.jctc.5b00057.  
23  
24  
25 (26) Mackerell, A. D. *J. Comput. Chem.* **2004**, *25*, 1584–1604.  
26  
27  
28 (27) Kwiatkowski, J. J.; Nelson, J.; Li, H.; Bredas, J. L.; Wenzel, W.; Lennartz, C. *Phys.*  
29 *Chem. Chem. Phys.* **2008**, *10*, 1852–1858.  
30  
31  
32 (28) Lukyanov, A.; Lennartz, C.; Andrienko, D. *Phys. Status Solidi (a)* **2009**, *206*, 2737–  
33 2742.  
34  
35  
36 (29) May, F.; Al-Helwi, M.; Baumeier, B.; Kowalsky, W.; Fuchs, E.; Lennartz, C.; An-  
37 drienko, D. *J. Am. Chem. Soc.* **2012**, *134*, 13818–13822.  
38  
39  
40 (30) Friederich, P.; Symalla, F.; Meded, V.; Neumann, T.; Wenzel, W. *J. Chem. Theory*  
41 *Comput.* **2014**, *10*, 3720–3725.  
42  
43  
44 (31) Tao, Y.; Yuan, K.; Chen, T.; Xu, P.; Li, H.; Chen, R.; Zheng, C.; Zhang, L.; Huang, W.  
45 *Adv. Mater.* **2014**, *26*, 7930–7930.  
46  
47  
48 (32) Adachi, C. *Jpn. J. Appl. Phys.* **2014**, *53*, 060101.  
49  
50  
51  
52  
53  
54  
55  
56  
57  
58  
59  
60

- 1  
2  
3  
4 (33) Jankus, V.; Data, P.; Graves, D.; McGuinness, C.; Santos, J.; Bryce, M. R.; Dias, F. B.;  
5 Monkman, A. P. *Adv. Funct. Mater.* **2014**, *24*, 6178–6186.  
6  
7  
8 (34) Moral, M.; Muccioli, L.; Son, W.-J.; Olivier, Y.; Sancho-García, J. C. *J. Chem. Theory*  
9 *Comput.* **2015**, *11*, 168–177.  
10  
11  
12 (35) Yu, M.; Wang, S.; Shao, S.; Ding, J.; Wang, L.; Jing, X.; Wang, F. *J. Mater. Chem. C*  
13 **2015**, *3*, 861–869.  
14  
15  
16 (36) Yuan, W. Z.; Gong, Y.; Chen, S.; Shen, X. Y.; Lam, J. W. Y.; Lu, P.; Lu, Y.; Wang, Z.;  
17 Hu, R.; Xie, N.; Kwok, H. S.; Zhang, Y.; Sun, J. Z.; Tang, B. Z. *Chem. Mater.* **2012**,  
18 *24*, 1518–1528.  
19  
20  
21 (37) Chemical drawings were generated by ChemSpider <http://www.chemspider.com> Ac-  
22 cessed date 04/20/2015.  
23  
24  
25 (38) Sasabe, H.; Kido, J. *Chem. Mater.* **2011**, *23*, 621–630.  
26  
27  
28 (39) Muccioli, L.; D'Avino, G.; Berardi, R.; Orlandi, S.; Pizzirusso, A.; Ricci, M.;  
29 Roscioni, O. M.; Zannoni, C. In *Multiscale Modelling of Organic and Hybrid Photo-*  
30 *voltatics*; Beljonne, D., Cornil, J., Eds.; Top. Curr. Chem.; Springer Berlin Heidelberg,  
31 2014; Vol. 352; pp 39–101.  
32  
33 (40) In this work, we enforced the united atom approximation also to the hydrogen attached  
34 to carbazole (CBZ) nitrogen (NH atom type in Table 1). This choice prevents the  
35 formation of a hydrogen bond: we discourage then the adoption of our force field for  
36 carbazole in presence of hydrogen bond acceptors.  
37  
38  
39 (41) Tiberio, G.; Muccioli, L.; Berardi, R.; Zannoni, C. *ChemPhysChem* **2009**, *10*, 125–136.  
40  
41  
42 (42) Vanommeslaeghe, K.; Hatcher, E.; Acharya, C.; Kundu, S.; Zhong, S.; Shim, J.; Dar-  
43 ian, E.; Guvench, O.; Lopes, P.; Vorobyov, I.; Mackerell, A. D. *J. Comput. Chem.* **2010**,  
44 *31*, 671–690.  
45  
46  
47  
48  
49  
50  
51  
52  
53  
54  
55  
56  
57  
58  
59  
60

- 1  
2  
3  
4 (43) Cornell, W. D.; Cieplak, P.; Bayly, C. I.; Gould, I. R.; Merz Jr., K. M.;erguson, D.  
5 M. F.; Spellmeyer, D. C.; Fox, T.; Caldwell, J. W.; Kollman, P. A. *J. Am. Chem. Soc.*  
6 **1995**, *117*, 5179.  
7  
8  
9  
10 (44) Pizzirusso, A.; Di Pietro, M. E.; De Luca, G.; Celebre, G.; Longeri, M.; Muccioli, L.;  
11 Zannoni, C. *ChemPhysChem* **2014**, *15*, 1356–1367.  
12  
13  
14  
15 (45) Reva, I.; Lapinski, L.; Chattopadhyay, N.; Fausto, R. *Phys. Chem. Chem. Phys.* **2003**,  
16 *5*, 3844–3850.  
17  
18  
19  
20 (46) Hénin, J.; Chipot, C. *J. Chem. Phys.* **2004**, *121*, 2904–2914.  
21  
22  
23 (47) Weiner, S. J.; Kollmann, P. A.; Case, D. A.; Singh, U. C.; Ghio, C.; Alagona, G.;  
24 Profeta, S.; Weiner, P. *J. Am. Chem. Soc.* **1984**, *106*, 765–784.  
25  
26  
27  
28 (48) Yang, L. J.; Tan, C. H.; Hsieh, M. J.; Wang, J. M.; Duan, Y.; Cieplak, P.; Caldwell, J.;  
29 Kollman, P. A.; Luo, R. *J. Phys. Chem. B* **2006**, *110*, 13166–13176.  
30  
31  
32  
33 (49) von Lilienfeld, O. A.; Andrienko, D. *J. Chem. Phys.* **2006**, *124*, 054307.  
34  
35  
36 (50) Wang, J.; Wolf, R. M.; Caldwell, J. W.; Kollman, P. A.; Case, D. A. *J. Comput. Chem.*  
37 **2004**, *25*, 1157.  
38  
39  
40 (51) Perdew, J. P.; Ernzerhof, M.; Burke, K. *J. Chem. Phys.* **1996**, *105*, 9982.  
41  
42  
43 (52) Perdew, J. P.; Burke, K.; Ernzerhof, M. *Phys. Rev. Lett.* **1996**, *77*, 3865–3868.  
44  
45  
46 (53) Zhang, Y.; Yang, W. *Phys. Rev. Lett.* **1998**, *80*, 890.  
47  
48  
49 (54) Adamo, C.; Barone, V. *J. Chem. Phys.* **1999**, *110*, 6158–6170.  
50  
51  
52 (55) Weigend, F.; Ahlrichs, R. *Phys. Chem. Chem. Phys.* **2005**, *7*, 3297–3305.  
53  
54  
55 (56) Grimme, S.; Ehrlich, S.; Goerigk, L. *J. Comput. Chem.* **2011**, *32*, 1456–1465.  
56  
57  
58 (57) Besler, B. H.; Merz Jr, K. M.; Kollman, P. A. *J. Comput. Chem.* **1990**, *11*, 431–439.  
59  
60

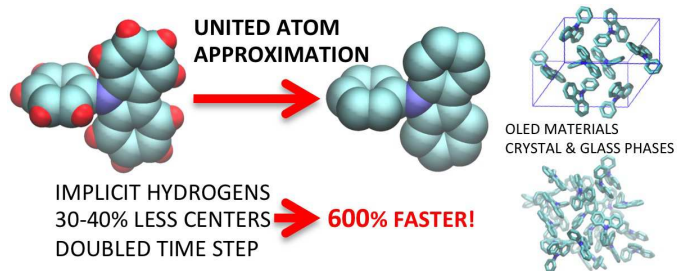
- 1  
2  
3  
4 (58) Frisch, M. J.; Trucks, G. W.; Schlegel, H. B.; Scuseria, G. E.; Robb, M. A.; Cheese-  
5 man, J. R.; Scalmani, G.; Barone, V.; Mennucci, B.; Petersson, G. A.; Nakatsuji, H.;  
6 Caricato, M.; Li, X.; Hratchian, H. P.; Izmaylov, A. F.; Bloino, J.; Zheng, G.; Sonnen-  
7 berg, J. L.; Hada, M.; Ehara, M.; Toyota, K.; Fukuda, R.; Hasegawa, J.; Ishida, M.;  
8 Nakajima, T.; Honda, Y.; Kitao, O.; Nakai, H.; Vreven, T.; Montgomery, J. A., Jr.;  
9 Peralta, J. E.; Ogliaro, F.; Bearpark, M.; Heyd, J. J.; Brothers, E.; Kudin, K. N.;  
10 Staroverov, V. N.; Kobayashi, R.; Normand, J.; Raghavachari, K.; Rendell, A.; Bu-  
11 rant, J. C.; Iyengar, S. S.; Tomasi, J.; Cossi, M.; Rega, N.; Millam, J. M.; Klene, M.;  
12 Knox, J. E.; Cross, J. B.; Bakken, V.; Adamo, C.; Jaramillo, J.; Gomperts, R.; Strat-  
13 mann, R. E.; Yazyev, O.; Austin, A. J.; Cammi, R.; Pomelli, C.; Ochterski, J. W.;  
14 Martin, R. L.; Morokuma, K.; Zakrzewski, V. G.; Voth, G. A.; Salvador, P.; Dan-  
15 nenberg, J. J.; Dapprich, S.; Daniels, A. D.; Farkas, J.; Foresman, J. B.; Ortiz, J. V.;  
16 Cioslowski, J.; Fox, D. J. Gaussian09 Revision A.01. Gaussian Inc. Wallingford CT  
17 2009.
- 18  
19  
20  
21  
22  
23  
24  
25  
26  
27  
28  
29  
30  
31  
32  
33 (59) Neese, F. *Wiley Interdiscip. Rev.-Comput. Mol. Sci.* **2012**, *2*, 73–78.
- 34  
35  
36 (60) Phillips, J. C.; Braun, R.; Wang, W.; Gumbart, J.; Tajkhorshid, E.; Villa, E.;  
37 Chipot, C.; Skeel, R. D.; Kale, L.; Schulten, K. *J. Comput. Chem.* **2005**, *26*, 1781–1802.
- 38  
39  
40 (61) The atom types CW and N5 were introduced to identify proper and improper dihedrals  
41 of PTBI. Apart this, they coincide with CY and N4 atom types.
- 42  
43  
44  
45 (62) Charbonneau, G. P.; Delugeard, Y. *Acta Crystallogr. Sect. B* **1977**, *33*, 1586–1588.
- 46  
47  
48 (63) Gerkin, R. E.; Reppart, W. J. *Acta Crystallogr. Sect. C* **1986**, *42*, 480–482.
- 49  
50  
51 (64) Belsky, V. K.; Zavodnik, V. E.; Vozzhennikov, V. M. *Acta Crystallogr. Sect. C* **1984**,  
52 *40*, 1210–1211.
- 53  
54  
55  
56 (65) Sun, Y.-H.; Zhu, X.-H.; Chen, Z.; Zhang, Y.; Cao, Y. *J. Org. Chem.* **2006**, *71*, 6281–  
57 6284.  
58  
59  
60

- 1  
2  
3  
4 (66) Low, P. J.; Paterson, M. A. J.; Yufit, D. S.; Howard, J. A. K.; Cherryman, J. C.;  
5 Tackley, D. R.; Brook, R.; Brown, B. *J. Mater. Chem.* **2005**, *15*, 2304–2315.  
6  
7  
8 (67) Woźniak, K.; Kariuki, B.; Jones, W. *Acta Crystallogr. Sect. C* **1991**, *47*, 1113–1114.  
9  
10  
11 (68) Avendano, C.; Espada, M.; Ocana, B.; Garcia-Granda, S.; Diaz, M.; Tejerina, B.;  
12 Gomez-Beltran, F.; Martinez, A.; Elguero, J. *J. Chem. Soc., Perkin Trans. 2* **1993**,  
13 1547–1555.  
14  
15  
16  
17  
18 (69) Sobolev, A. N.; Belsky, V. K.; Romm, I. P.; Chernikova, N. Y.; Guryanova, E. N. *Acta*  
19 *Crystallogr. Sect. C* **1985**, *41*, 967–971.  
20  
21  
22  
23 (70) In the case of a relatively small isotropic box deformation  $l_s^i = \lambda l_e^i$ , or  $l_s^i = (1+x)l_e^i$   
24 with  $x = \lambda - 1$  and  $|x| \ll 1$ ,  $F$  becomes approximately equal to  $|x|$ .  
25  
26 In fact for this particular case  $V_s = (1+x)^3 V_e$ ,  $\Delta_{vol} = (1/3)|V_e - V_e(1+x)^3|/V_e =$   
27  $(1/3)|3x + 3x^2 + x^3|$ , and  $\Delta_{def} = (1/3)(3|x| + 3|x|^2 + 3|x|^3)$ . For small  $|x|$  hence we have  
28  $\Delta_{vol}$  and  $\Delta_{def} \simeq |x|$ , and of course  $F = 1/2(\Delta_{vol} + \Delta_{def}) \simeq |x|$ .  
29  
30  
31  
32  
33  
34 (71) D'Avino, G.; Muccioli, L.; Zannoni, C.; Beljonne, D.; Soos, Z. G. *J. Chem. Theory*  
35 *Comput.* **2014**, *10*, 4959–4971.  
36  
37  
38  
39 (72) Jurečka, P.; Černý, J.; Hobza, P.; Salahub, D. R. *J. Comput. Chem.* **2007**, *28*, 555–569.  
40  
41  
42 (73) Grimme, S. *WIREs Comput. Mol. Sci.* **2011**, *1*, 211–228.  
43  
44  
45 (74) Sherrill, C. D. *Acc. Chem. Res.* **2013**, *46*, 1020–1028.  
46  
47  
48 (75) Sherrill, C. D.; Sumpter, B. G.; Sinnokrot, M. O.; Marshall, M. S.; Hohenstein, E. G.;  
49 Walker, R. C.; Gould, I. R. *J. Comput. Chem.* **2009**, *30*, 2187–2193.  
50  
51  
52 (76) Olivier, Y.; Muccioli, L.; Zannoni, C. *ChemPhysChem* **2014**, *15*, 1345–1355.  
53  
54  
55 (77) Pettersson, I.; Liljefors, T. *J. Comput. Chem.* **1987**, *8*, 1139–1145.  
56  
57  
58 (78) Jorgensen, W. L.; Tirado-Rives, J. *J. Am. Chem. Soc.* **1988**, *110*, 1657–1666.  
59  
60

- 1  
2  
3  
4 (79) Olivier, Y.; Muccioli, L.; Lemaire, V.; Geerts, Y. H.; Zannoni, C.; Cornil, J. *J. Phys.*  
5 *Chem. B* **2009**, *113*, 14102–14111.  
6  
7  
8 (80) D'Avino, G.; Mothy, S.; Muccioli, L.; Zannoni, C.; Wang, L.; Cornil, J.; Beljonne, D.;  
9 Castet, F. *J. Phys. Chem. C* **2013**, *117*, 12981–12990.  
10  
11  
12 (81) Agrawal, P. M.; Rice, B. M.; Thompson, D. L. *J. Chem. Phys.* **2003**, *118*, 9680–9688.  
13  
14  
15 (82) Zhang, Y.; Maginn, E. J. *J. Chem. Phys.* **2012**, *136*, 144116.  
16  
17  
18 (83) Marcon, V.; Raos, G. *J. Am. Chem. Soc.* **2006**, *128*, 1408–1409.  
19  
20  
21 (84) Massaro, F. R.; Moret, M.; Bruno, M.; Aquilano, D. *Cryst. Growth & Des.* **2013**, *13*,  
22 1334–1341.  
23  
24  
25 (85) Rohl, A.; Gay, D. *J. Cryst. Growth* **1996**, *166*, 84 – 90.  
26  
27  
28 (86) Experimental melting points were obtained from Sigma Aldrich online catalogue  
29 <http://www.sigmaaldrich.com/catalog/> Accessed date 04/20/2015.  
30  
31  
32 (87) Vydrov, O. A.; Van Voorhis, T. *J. Chem. Phys.* **2010**, *133*, 244103.  
33  
34  
35 (88) Sure, R.; Grimme, S. *J. Comput. Chem.* **2013**, *34*, 1672–1685.  
36  
37  
38 (89) Sinnokrot, M. O.; Sherrill, C. D. *J. Phys. Chem. A* **2004**, *108*, 10200–10207.  
39  
40  
41 (90) Yang, J.; Hu, W.; Usvyat, D.; Matthews, D.; Schtz, M.; Chan, G. K.-L. *Science* **2014**,  
42 *345*, 640–643.  
43  
44  
45 (91) Worle, M.; Losio, P. A.; Gunter, P. *private communication* **2006**, CCDC 298742 REH-  
46 JAQ01.  
47  
48  
49 (92) Song, W.-F.; Wu, Y.; Fan, Y.; Wang, Y.; Liu, Y. *Acta Crystall. Sect. E* **2009**, *65*,  
50 o2461.  
51  
52  
53 (93) Peter, C.; Kremer, K. *Faraday Discuss.* **2010**, *144*, 9–24.  
54  
55  
56  
57  
58  
59  
60

- 1  
2  
3  
4 (94) Carbone, P.; Varzaneh, H. A. K.; Chen, X.; Müller-Plathe, F. *J. Chem. Phys.* **2008**,  
5 *128*, 064904.  
6  
7  
8 (95) Hofmann, D. W. M.; Kuleshova, L. N. *Cryst. Growth Des.* **2014**, *14*, 3929–3934.  
9  
10  
11  
12  
13  
14  
15  
16  
17  
18  
19  
20  
21  
22  
23  
24  
25  
26  
27  
28  
29  
30  
31  
32  
33  
34  
35  
36  
37  
38  
39  
40  
41  
42  
43  
44  
45  
46  
47  
48  
49  
50  
51  
52  
53  
54  
55  
56  
57  
58  
59  
60

## Table of content graphic



1  
2  
3  
4  
5  
6  
7  
8  
9  
10  
11  
12  
13  
14  
15  
16  
17  
18  
19  
20  
21  
22  
23  
24  
25  
26  
27  
28  
29  
30  
31  
32  
33  
34  
35  
36  
37  
38  
39  
40  
41  
42  
43  
44  
45  
46  
47  
48  
49  
50  
51  
52  
53  
54  
55  
56  
57  
58  
59  
60